The Astronomical Journal, 154:178 (12pp), 2017 November https://doi.org/10.3847/1538-3881/aa899d

D/H Ratios on Saturn and Jupiter from *Cassini* CIRS

J. D. R. Pierel[1,2,7], C. A. Nixon[1], E. Lellouch[3], L. N. Fletcher[4], G. L. Bjoraker[1], R. K. Achterberg[1,5], B. Bézard[3], B. E. Hesman[1,5], P. G. J. Irwin[6], and F. M. Flasar[1]

[1] Planetary Systems Laboratory, NASA Goddard Space Flight Center, Greenbelt, MD 20771, USA
[2] Department of Physics, University of Maryland, Baltimore, MD 21250, USA
[3] LESIA-Observatoire de Paris, CNRS, UPMC, Université Paris–Diderot, 5 place Jules Janssen, F-92195 Meudon, France
[4] Department of Physics & Astronomy, University of Leicester, University Road, Leicester, LE1 7RH, UK
[5] University of Maryland, College Park, MD 20742, USA
[6] Department of Physics, Atmospheric, Oceanic and Planetary Physics, University of Oxford, Oxford OX1 3PU, UK
Received 2017 May 25; revised 2017 August 28; accepted 2017 August 29; published 2017 October 5

Abstract

We present new measurements of the deuterium abundance on Jupiter and Saturn, showing evidence that Saturn's atmosphere contains less deuterium than Jupiter's. We analyzed far-infrared spectra from the *Cassini* Composite Infrared Spectrometer to measure the abundance of HD on both giant planets. Our estimate of the Jovian $D/H = (2.95 \pm 0.55) \times 10^{-5}$ is in agreement with previous measurements by *ISO*/SWS: $(2.25 \pm 0.35) \times 10^{-5}$, and the Galileo probe: $(2.6 \pm 0.7) \times 10^{-5}$. In contrast, our estimate of the Saturn value of $(2.10 \pm 0.13) \times 10^{-5}$ is somewhat lower than on Jupiter (by a factor of $0.71^{+0.22}_{-0.15}$), contrary to model predictions of a higher ratio: Saturn/Jupiter = 1.05–1.20. The Saturn D/H value is consistent with estimates for hydrogen in the protosolar nebula $(2.1 \pm 0.5) \times 10^{-5}$, but its apparent divergence from the Jovian value suggests that our understanding of planetary formation and evolution is incomplete, which is in agreement with previous work.

Key words: infrared: planetary systems – planets and satellites: atmospheres – planets and satellites: composition – planets and satellites: formation – planets and satellites: gaseous planets

1. Introduction

Accurate determinations of the deuterium to hydrogen (D/H) ratio in the giant planets provide fundamental constraints for modeling planetary formation and evolution (Hersant et al. 2001). Previous determinations of D/H in the contemporary Local Interstellar Medium (LISM) suggest an average value today of $(1.5 \pm 0.1) \times 10^{-5}$ (Linsky 1998), and the protosolar value, derived from measurements of ^{3}He in the solar wind and corrected for protosolar ^{3}He using the ^{3}He/^{4}He ratio in meterorites, is $(2.1 \pm 0.5) \times 10^{-5}$ (Geiss & Gloecker 1998; Lellouch et al. 2001). This decrease in D/H over time from the protosolar value to the LISM value is anticipated, as deuterium is destroyed during nucleosynthesis in stars including the Sun (Griffin et al. 1996; Ferlet & Lemoine 1998; Lellouch et al. 2001). It is expected that Jupiter and Saturn will exhibit D/H ratios at or above the protosolar value as the bulk of the deuterium in both planets should have come from hydrogen in the primordial nebula, with some enrichment possible due to the mixing of atmosphere with protoplanetary embryos comprised of deuterium-enriched ices (Lellouch et al. 2001). However, Saturn is expected to have a slightly higher D/H than Jupiter, due to a larger core-to-envelope ratio (Guillot 1999a).

While an in situ measurement of Jupiter's atmosphere was obtained by the Galileo probe: $D/H = (2.6 \pm 0.7) \times 10^{-5}$ (Mahaffy et al. 1998), there has yet to be a similar probe mission and corresponding in situ measurement of the D/H ratio on Saturn. Although earlier measurements from infrared remote sensing have suggested that the D/H ratio on Saturn may be smaller than that on Jupiter (Griffin et al. 1996; Lellouch et al. 2001; Fletcher et al. 2009b), the uncertainties on direct measurements in H_2were large enough that the values on the two gas giants were still consistent with one another. This study tightens the constraints on the Saturnian D/H by analyzing far-infrared spectra from the *Cassini* Composite Infrared Spectrometer (CIRS) instrument on board the *Cassini* spacecraft to measure HD.

2. Observations

CIRS is a hybrid instrument, comprised of separate mid- and far-infrared (IR) interferometers that share a common telescope, scan mechanism, reference laser, and other components, but with distinct lightpaths from the telescope to the focal planes. The far-IR instrument has a single thermopile pixel (FP1) operating at the instrument temperature, 170 K, and is sensitive from 10 to 600 cm^{-1}. The mid-infrared focal plane is comprised of two 1×10 HgCdTe detector arrays: FP3 (600–1100 cm^{-1}) and FP4 (1100–1400 cm^{-1}). The spectral resolution is the same on both instruments and is set by the scan mirror travel distance, with a maximum resolution (smallest FWHM) of 0.5 cm^{-1}. For more details on the CIRS instrument, see Flasar et al. (2004) and Jennings et al. (2017).

2.1. Saturn

Cassini has been orbiting Saturn since 2004 July, but this analysis uses only data from 2004 to 2009 in order to avoid the well documented effects of the great Saturn storm that arose in 2010 (Achterberg et al. 2014). Data for the CIRS Saturn analysis were taken from the CIRS v4.2 calibrated data set, using observations with emission angles below 30° (Table 1). CIRS far-infrared (FP1) data were selected in the spectral range ~35–400 cm^{-1}, and the primary HD rotational transition visible in the CIRS spectra was R(1) at 177.84 cm^{-1} (Figures 1, 2). The partial derivative, $\frac{\partial L\nu}{\partial x_i}$, of the spectral radiance with respect to perturbations of a model parameter, x_i,

[7] Now at Department of Physics and Astronomy, University of South Carolina, Columbia, SC 29208, USA.

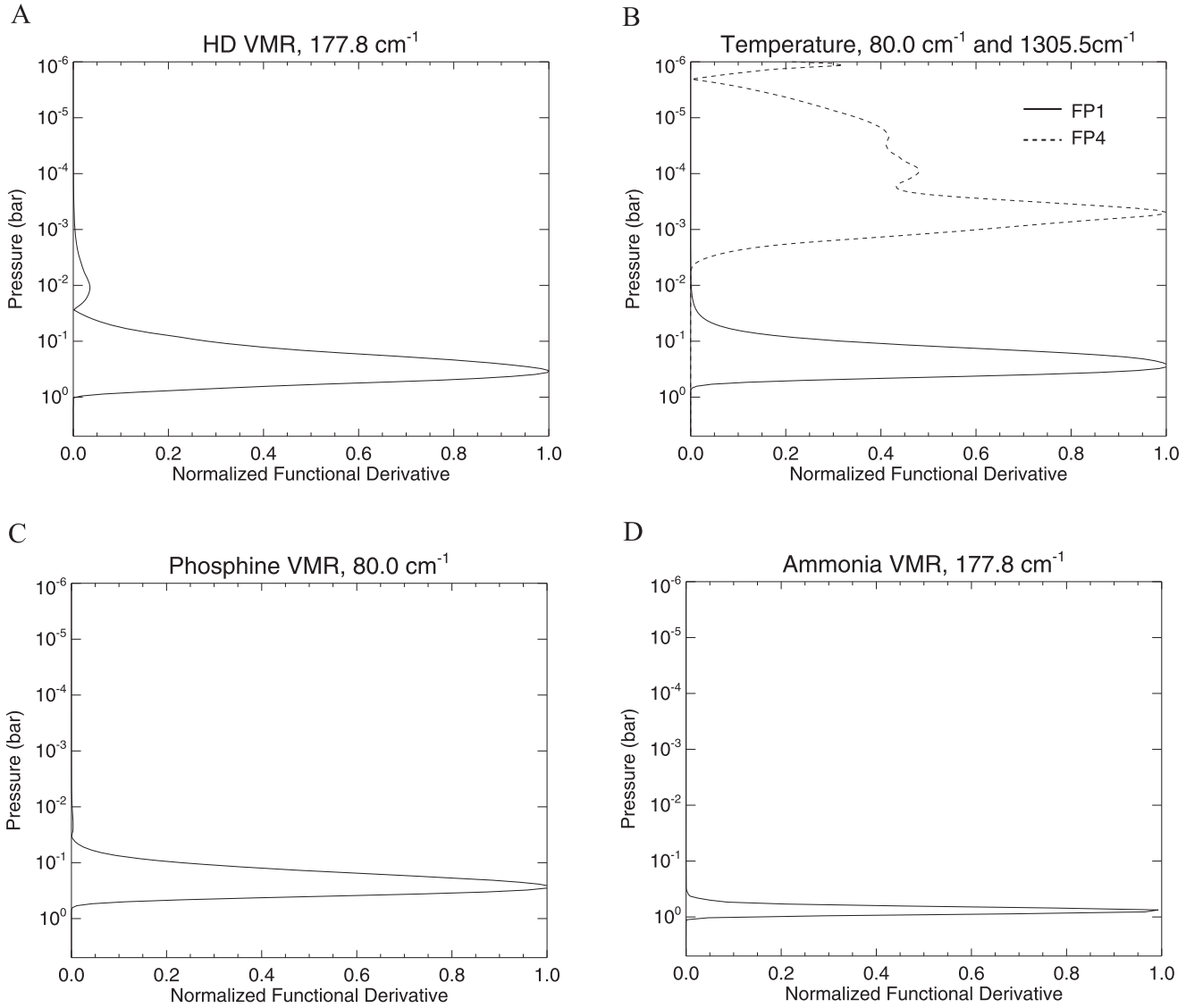

Figure 1. Functional derivatives for (A) HD volume mixing ratio (VMR) at R(1) (177.8 cm^{-1}) in Saturn's atmosphere, showing a peak at ∼0.3 bar and a small stratospheric contribution; (B) temperature at 80.0 cm^{-1} (solid) and 1305.5 cm^{-1} (dashed), with peaks at ∼0.2 bar and ∼0.7 mbar, respectively (Figure 1(B)); (C) PH_3 VMR at 80.0 cm^{-1}, showing a peak at ∼0.2 bar; (D) NH_3 VMR at R(1) (178.8 cm^{-1}), with a peak at ∼0.8 bar. All functional derivatives were calculated at the highest (0.25 cm^{-1} unapodized) spectral resolution of CIRS.

at each pressure level is called the functional derivative. Functional derivatives for modeled species (Figure 1) showed that despite a small stratospheric contribution for HD, temperature information from FP1 was sufficient for an accurate retrieval. The use of mid-infrared (FP4) data to gain stratospheric temperature information was explored, but the FP4 functional derivative for temperature showed a negligible overlap with that of HD (Figures 1(A)–(B)). Electrical inferences from the instrument (Chan et al. 2015) and other spectral ranges of known high error were removed from the FP1 data.

2.2. Jupiter

For the CIRS Jupiter analysis, FP1 data in the spectral range 50–360 cm^{-1} were selected from the CIRS v3.2 data version, recorded during the *Cassini* flyby from 2000 December 13 through 2001 January 13. These dates permitted 832 spectra covering all latitudes to be used in the average, allowing the measurement of a single global D/H value for Jupiter.

Table 1
Details of CIRS Saturn Spectral Averages Modeled in This Analysis

Latitude	Emission Angle	Number of Spectra in Average
65.5 N	9.°1	1445
50.5 N	10.°8	1323
41.1 N	12.°3	1234
24.2 N	18.°3	1366
0.9 N	16.°3	1032
13.8 S	18.°5	1059
56.6 S	12.°6	1196

Note. All spectra are from CIRS FP1 in the spectral range 50–360 cm^{-1}.

3. Methodology

3.1. Atmospheric Modeling

This work used the Nonlinear Optimal Estimator for Multivariate Spectral Analysis (NEMESIS) retrieval algorithm

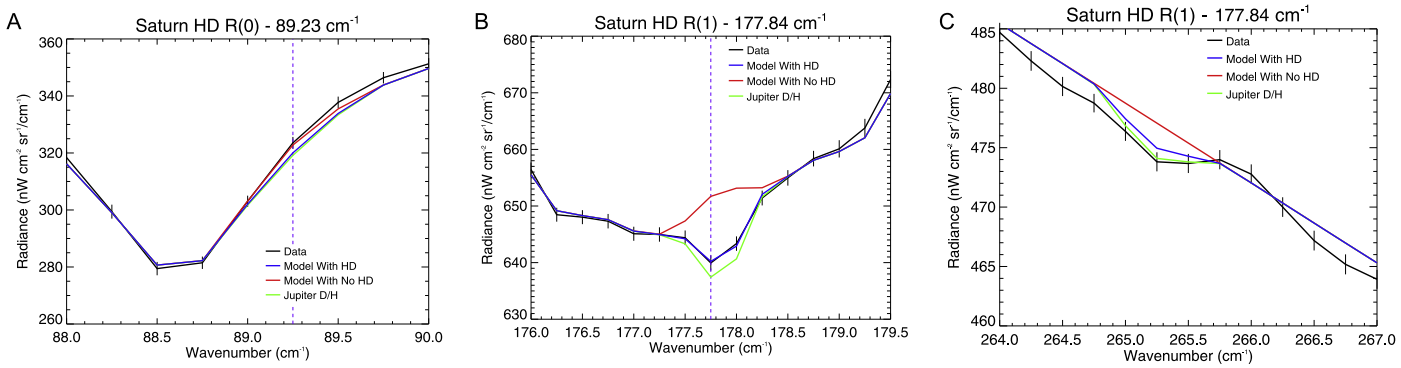

Figure 2. The R(0), R(1), and R(2) rotational transitions of HD on Saturn, with peak absorption locations represented by purple dotted lines. The R(0) and R(1) lines are found on the edge of a PH_3 absorption and within a strong NH_3 absorption, respectively. The R(1) line is strongest for Saturn, and the R(3) line at 350.85 cm^{-1} is not shown due to high spectral noise, preventing derivation of any useful constraints. Black line: CIRS data (with 1σ error bars). Colored lines: NEMESIS models with different HD mole fractions. Red: no HD. Blue: best-fit model containing an HD mole fraction of 3.69×10^{-5}. Green: calculation using an HD mole fraction of 5.17×10^{-5}, equal to the new CIRS measurement for Jupiter. Models with no HD and Jupiter HD do not fit the R(1) data to within error bars.

Table 2
HD Line Parameters Used for Saturn and Jupiter CIRS Analysis (for Details, see Feuchtgruber et al. 2013)

Line	ν[a] (cm^{-1})	Line Intensity[b] (cm^{-1}/(molec cm^{-2}))	γ[b] (cm^{-1}/atm)	E_{Lower} (cm^{-1})	n[b]	δ[b] (cm^{-1}/atm)
R(0)	89.227951	1.769×10^{-24}	0.013	0.000	−0.23	0.0180
R(1)	177.841797	7.517×10^{-24}	0.010	89.228	0.20	0.0130
R(2)	265.241119	8.870×10^{-24}	0.008	267.070	0.13	0.0110
R(3)	350.852936	4.867×10^{-24}	0.009	532.311	−0.03	0.0080

Notes.
[a] Rothman et al. (2013).
[b] Feuchtgruber et al. (2013).

for our radiative transfer code (Irwin et al. 2008). The accuracy and reliability of using NEMESIS for the interpretation of observed spectra from the *Cassini* mission, both on Saturn and Jupiter, is extremely well documented (e.g., Nixon et al. 2007; Fletcher et al. 2010). The NEMESIS retrieval algorithm operates by computing a goodness-of-fit metric ϕ, called the cost function, for a forward model. The cost function is essentially a modified chi-squared test between model and data, but additionally includes a constraint from a priori information about the likely range of values a parameter can take. Once the cost function is computed, the algorithm calculates $\frac{\partial \phi}{\partial x_i}$, or the derivative of the cost function ϕ with respect to each of the retrieved quantities. Finally, the state vector is modified iteratively until a pre-set convergence limit is reached in order to minimize ϕ. For more details about the NEMESIS algorithm, see Irwin et al. (2008).

Model atmospheres were initialized for Jupiter and Saturn using a priori temperature and gas information from previous work, Fletcher et al. (2009) for Saturn and Nixon et al. (2010) for Jupiter. Equilibrium para-H_2 fraction was calculated as a function of the a priori temperature profiles described above and then retrieved as a full vertical profile along with temperature over a pressure range of ~10 bar-1 μbar. The vertical profile of methane was initialized for Saturn and Jupiter using vertical profiles from Fletcher et al. (2009) and then held constant during all FP1 retrievals. PH_3 and NH_3volume mixing ratios (VMRs) were parameterized by Equation (1):

$$X = X_0 \left(\frac{p}{p_0} \right)^{\frac{1}{f}-1} \quad (1)$$

where X is the species abundance and is a function of pressure p, X_0 is the deep concentration (VMR), p_0 is the "knee" pressure signifying the transition level from deep fixed abundance to varying abundance, and f is the fractional scale height that decreases the abundance above the "knee" level (Hurley et al. 2012). The value of p_0 is fixed for each latitude bin, but a small range of pressures near established literature values (Fletcher et al. 2009a, 2010) were tested in the modeling process. For Saturn, the average values of p_0 used for PH_3 and NH_3 are 580 mbar and 900 mbar, respectively, compared with literature values of 550 mbar and 1 bar, respectively. Jupiter uses a value of 1 bar for PH_3 (Fletcher et al. 2009a) and 850 mbar for NH_3 (Fletcher et al. 2014). Equation (2) was used to calculate the H_2 mole fraction

$$\frac{[He]}{[H_2]} = \frac{1 - [H_2] - [CH_4]}{[H_2]} \quad (2)$$

where Hydrogen and Helium were taken to be uniformly mixed setting $He/H_2 = 0.135 \pm 0.025$ for Saturn (Conrath & Gautier 2000), and $He/H_2 = 0.1359 \pm 0.0027$ for Jupiter (Von Zahn et al. 1998). In all analyses, the HD mole fraction was measured, providing a means by way of Equation (3) of calculating the D/H ratio in H_2

$$\frac{D}{H} = \frac{1}{2} * \frac{[HD]}{[H_2]} \quad (3)$$

where [HD] and $[H_2]$ are the mole fractions of HD and H_2, respectively. Previous attempts to include an aerosol profile on Saturn resulted in a worsened χ^2 value; therefore, this work

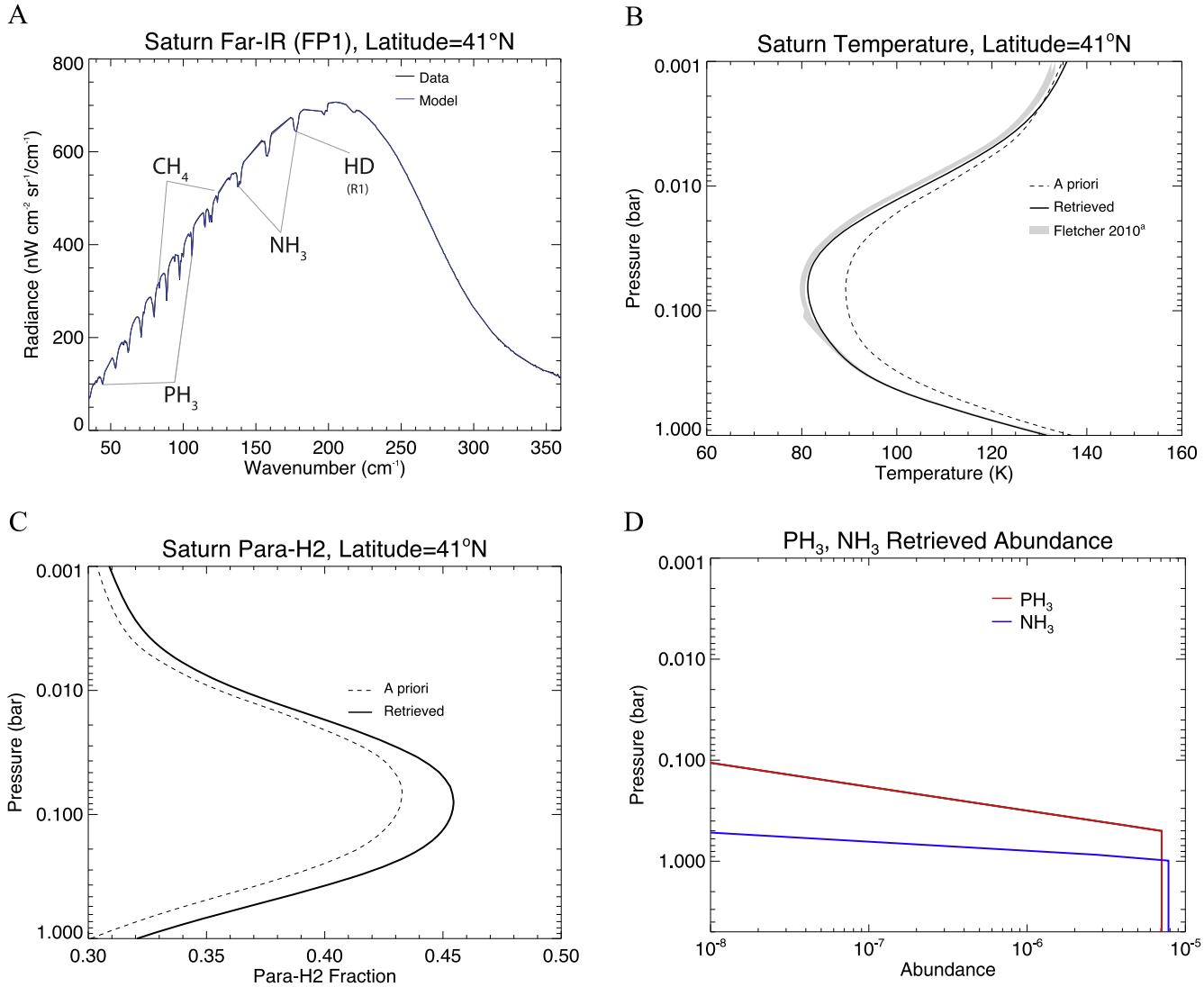

Figure 3. NEMESIS fitting to the Saturn CIRS far-IR spectral data (A). Temperature (B) and Para-H_2 fraction (C) were retrieved using continuous vertical profiles, and the temperature information derived in Fletcher et al. (2010) is superimposed upon the profile measured in this analysis for comparison, showing excellent agreement. PH_3 and NH_3 were retrieved using a three-parameter model (Equation (2)). Retrieved abundances of NH_3 and PH_3 are shown in (D). Once an optimum fit was achieved for the modeled species in FP1 data, a series of forward models were run in order to determine the correct abundance of HD (Figure 4; Fletcher et al. 2010).

uses a cloud-free atmospheric profile throughout all modeling processes (Fletcher 2007).

Generating line-by-line synthetic spectra for NEMESIS is computationally expensive; therefore, correlated-*k* distributions were constructed to calculate line opacities. The correlated-*k* method creates a smooth function of the absorption coefficients that is readily integrated, which significantly reduced computational time (Lacis & Oinas 1991). Both the retrieval and forward model capabilities of Nemesis were used to generate atmospheric models and measure gas abundances on Jupiter and Saturn from CIRS spectra.

The HD line parameters used to generate correlated-*k* distributions for the CIRS analyses (Table 2) were derived in Feuchtgruber et al. (2013) Section 3, where a detailed explanation of their origin is given. For details on the various line parameters used in the *ISO*/SWS reanalysis, see Section 3.3. The correlated-*k* distributions created for the other gases included in the modeling efforts were generated from the HITRAN 2012 spectroscopic database (Rothman et al. 2013).

3.2. CIRS Data Modeling

3.2.1. Saturn

First, CIRS spectra with low emission angles were averaged in ∼15° latitude bins (Table 1). Next, the gas and temperature profiles for FP1 in the spectral range 50–360 cm^{-1} were retrieved using the NEMESIS retrieval algorithm. There are four rotational transitions [R(0), R(1), R(2), R(3)] of HD within the range of the CIRS FP1, though high spectral noise at R(3) renders the data unusable. Sensitivity at rotational transitions R(0) and R(2) is very close to the noise level (∼1–2σ), while R(1) at 177.84 cm^{-1} has a strong (∼9σ) feature in the CIRS spectra. Therefore, R(1) is the focus of this work, as it is the only rotational transition with sufficient sensitivity for modeling (Figure 2).

The methodology of this analysis corresponding to 41°N, shown in Figures 3(A)–(D), was repeated for seven latitude bins from 65.5°N to 44.5°S (Table 1, Figure 4). The CH_4 profile from Fletcher et al. (2009b) was used a priori and fixed

for all FP1 retrievals. Para-H_2 and temperature were retrieved using continuous vertical profiles (Figures 3(C)–(D)), while PH_3 and NH_3 were parameterized by a three-parameter model detailed in Equation (1) (Figure 3(E)). For details on these parameterizations, see Section 3.1. The R(1) rotational transition on Saturn is found within an NH_3 absorption, making it essential to accurately parameterize NH_3 before fitting the HD feature. Once an optimum fit was achieved for the temperature, para-H_2 fraction, NH_3, and PH_3 (Figure 3) over the full spectral range (50–360 cm^{-1}, 0.5 cm^{-1} spectral resolution), a series of localized forward models (168–183 cm^{-1}) were run using CIRS unapodized data (0.25 cm^{-1} spectral resolution) in order to determine the abundance of HD at R(1) (Figure 4).

3.2.2. Jupiter

Retrievals using CIRS data from the *Cassini* flyby of Jupiter were performed using the same process as for Saturn (see Section 3.2.1). As with Saturn, high spectral noise at R(3) renders the data unusable. Sensitivity at rotational transitions R(0) and R(1) is very close to the noise level ($\sim$0–1σ), while R(2) at 265.24 cm^{-1} has a much stronger ($\sim$6σ) feature in the CIRS spectra. Therefore, R(2) is the focus of this work, as it is the only rotational transition with sufficient sensitivity for modeling (Figure 5).

Fitting to the full CIRS FP1 data are shown in Figure 6(A). PH_3 and NH_3 were parameterized using the same methods, and all species as well as temperature and para-H_2 fraction were retrieved in the same way as for Saturn (Figures 6(B)–(D)). Once again, CH_4 abundance was held constant during all FP1 modeling. The retrievals using NEMESIS were computed using a disk-average in order to account for the large footprint of FP1 on Jupiter (Flasar et al. 2004). Unlike the Saturn analysis, for which it was possible to make measurements at different latitudes and average over 1000 spectra per latitude bin due to the much larger data set, our selected CIRS Jovian data set had an average of 832 spectra and only allowed the determination of a single D/H value for the planet. However, no latitude variation is expected, and indeed the Saturn analysis showed no significant latitude variation of D/H within the error bars (see Section 4.1.1). A cloud-free model was also used on Jupiter, both in order to remain consistent with the Saturn analysis, and because disc-averaging makes deriving cloud parameters meaningless. Unlike HD, clouds are highly latitude-dependent on Jupiter, so this uncertainty is effectively included in the systematic modeling error.

3.3. ISO/SWS

To validate the methodology and to allow deeper inter-comparison with previous work, a reanalysis of *ISO*/SWS data was performed to substantiate the use of the NEMESIS model for retrievals of HD abundance on Saturn. This work intentionally duplicated the modeling efforts of Lellouch et al. (2001), hereafter L01, which measured D/H on Saturn using *ISO*/SWS observations from 1996 January to 1997 December. Only the *ISO*/SWS grating data were used, which provided a spectral resolving power of $R \sim 1000$–2200 and allowed for fitting of the R(2) rotational transition at 37.7 μm (265.24 cm^{-1}). First, the line parameters derived in L01 were used in order to confirm that our radiative transfer code could reproduce the results of L01. Next, the data were reanalyzed using the updated values used in the CIRS work to allow for direct comparison (Tables 2, 3). The original L01 analysis tested a variety of cases for the thermal profile of Saturn, including the inclusion and exclusion of cloud opacity, and the consideration of warm and cold profiles by scaling the observed spectra by $\pm$15% to account for uncertainties on the thermal profile associated with absolute calibration uncertainties. Here, we have reanalyzed the *ISO* grating data using the same methodology as L01, but using only their cloud-free, nominal thermal profile.

As described in L01, there are a series of uncertainties in the *ISO*/SWS grating mode data that affected modeling, which were all accounted for in the current modeling effort. However, HD abundance retrievals from NEMESIS were not possible due to uncertainties in the absolute flux calibration as well as unreliable slope of the grating data continuum near the R(2) rotational transition. Therefore, forward modeling and line-to-continuum ratio comparisons are used by L01 and this work to calculate HD abundance. First, forward models of the H_2 quadrupole lines S(0) at 354.37 cm^{-1} and S(1) at 587.03 cm^{-1} using the cloud-free temperature profile information from L01 confirmed that our radiative transfer code is able to duplicate the fitting of these emissions (Figures 7(A)–(B)). *ISO*/SWS grating mode data also had an issue with continuum "leakage," which was accounted for in the modeling of the quadrupole lines by rescaling the line-to-continuum ratios by 20% and 10% for S(0) and S(1), respectively. After confirming the ability to duplicate the methods and results of L01 with the quadrupole lines, forward models were used to calculate the HD abundance from the R(2) line (Figure 7(C)). The *ISO*/SWS grating data were rescaled to match the NEMESIS model continuum, to correct for both the incorrect flux level and continuum slope, prior to fitting of the HD absorption. The original 2001 analysis determined the best-fit HD abundance by matching the absorption area of the model to the absorption area of the data, while this analysis determined HD abundance using a minimum χ^2.

4. Results

4.1. CIRS

The results of this analysis can be seen in Table 4 for both Saturn (PH_3, NH_3, and HD abundance; PH_3 and NH_3 fractional scale height [f.s.h.]) and Jupiter (HD abundance; PH_3 and NH_3 f.s.h.).

4.1.1. Saturn

In order to properly weight the data points (χ_i) by the reciprocal of their respective variances (σ_i), Equations (4) and (5) were used to calculate the mean (μ) and error (σ) respectively.

$$\mu = \frac{\sum(x_i/\sigma_i)}{\sum(1/\sigma_i^2)} \tag{4}$$

$$\sigma_\mu^2 = \frac{1}{\sum(1/\sigma_i^2)}. \tag{5}$$

The error calculation includes the spectral fitting error bar (σ) calculated by NEMESIS, the uncertainty in the line intensities given by Feuchtgruber et al. (2013), and the uncertainties in the hydrogen abundance ($He/H_2 = 0.135 \pm 0.025$, Conrath &

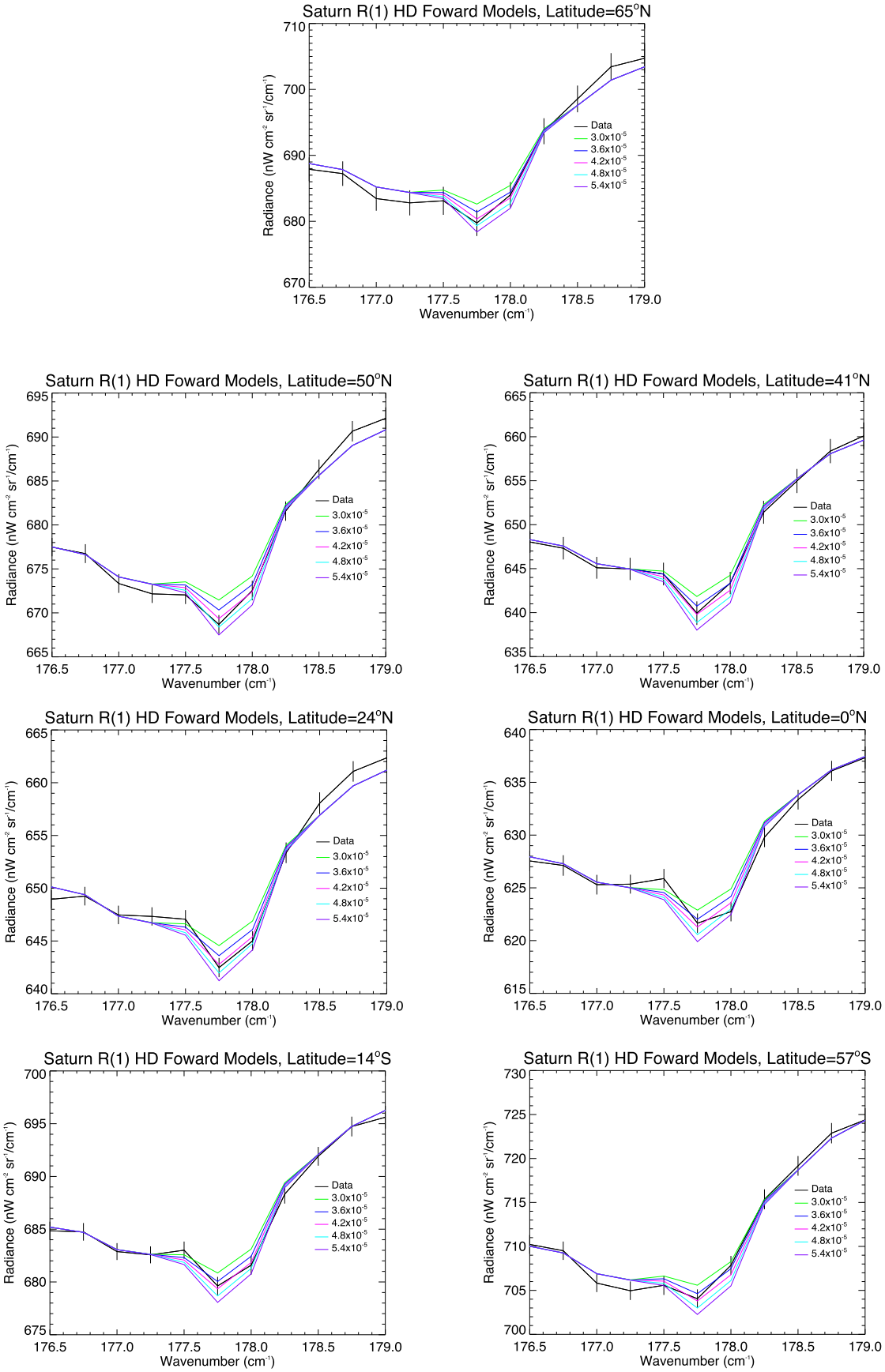

Figure 4. Results of forward modeling of the R(1) HD absorption at 177.84 cm^{-1} for all CIRS data latitude bins (Table 1). The colored lines represent differing mole fractions of HD, and the spectral data with error bars are in black.

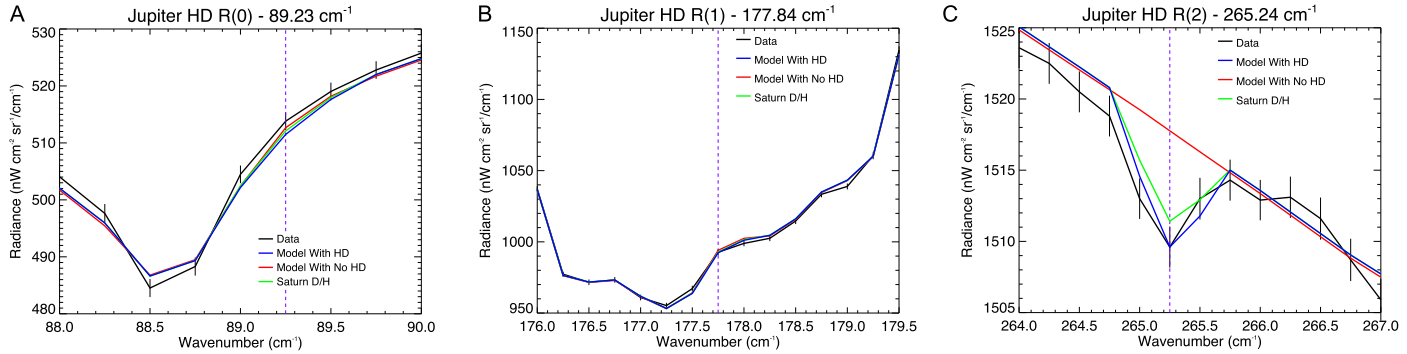

Figure 5. The R(0), R(1), and R(2) rotational transitions of HD on Jupiter, with peak absorption locations represented by purple dotted lines. The R(0) line and R(1) features are found on the edge of a PH_3 absorption and within a strong NH_3 absorption, respectively. The strongest absorption for Jupiter is R(2) (C), which is the focus of this work, and the R(3) line at 350.85 cm^{-1} is not shown due to high spectral noise, preventing derivation of any useful constraints. Black line: CIRS data (with 1σ error bars). Colored lines: NEMESIS models with different HD mole fractions. Red: no HD. Blue: best-fit model containing an HD mole fraction of 5.17×10^{-5}. Green: calculation using an HD mole fraction of 3.69×10^{-5}, equal to the new CIRS measurement for Saturn. Models with no HD and Saturn HD do not fit the data at R(2) to within error bars.

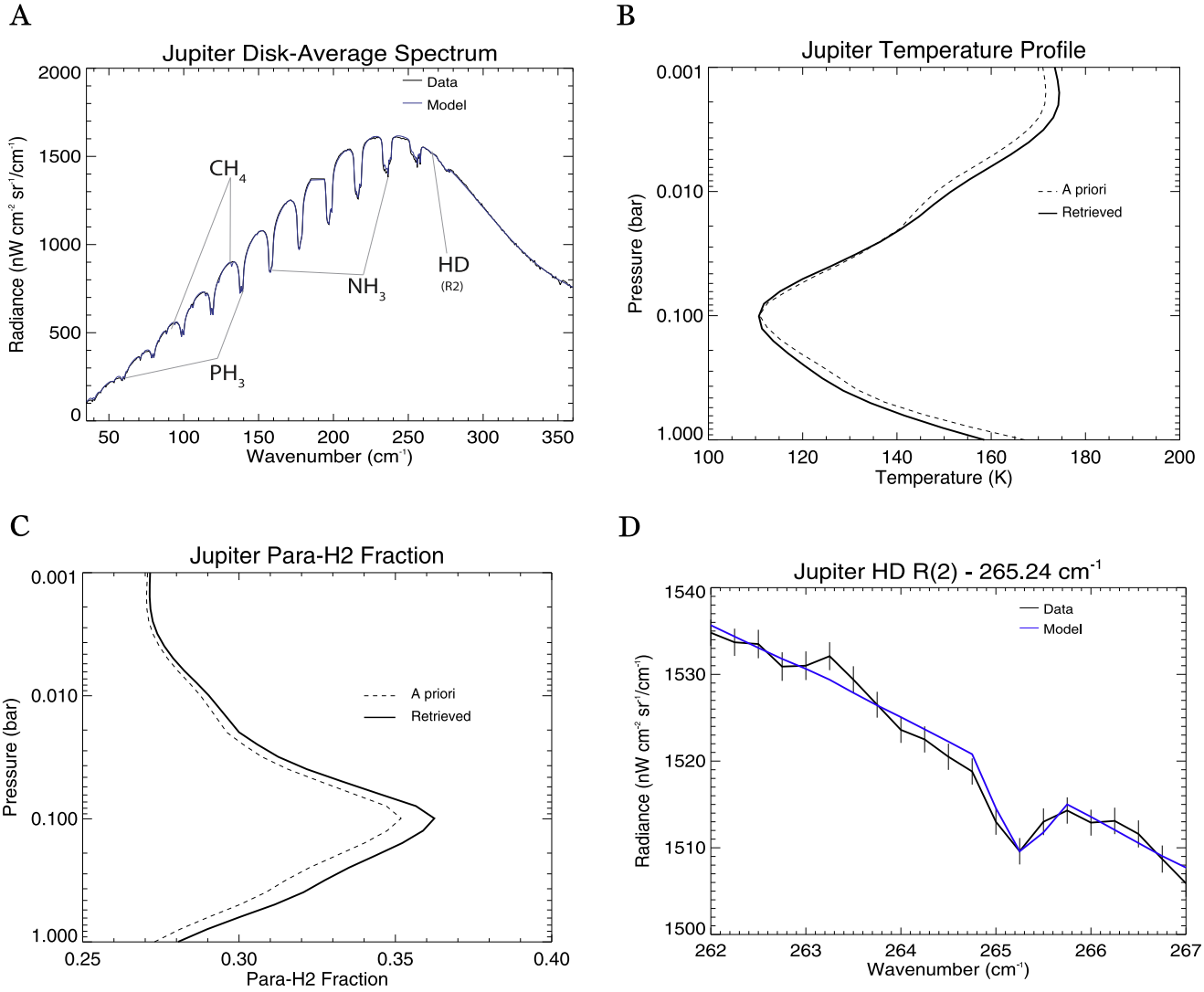

Figure 6. NEMESIS fitting to the CIRS Jupiter far-IR spectral data (A). Temperature and Para-H_2 fraction were retrieved using continuous vertical profiles (B), (C). Once a satisfactory fit was achieved for the spectral range 230–290 cm^{-1}, and particularly near the R(2) HD rotational transition at 265.24 cm^{-1}(D), a series of forward models were run in order to determine the correct abundance of HD (Figure 5(C)).

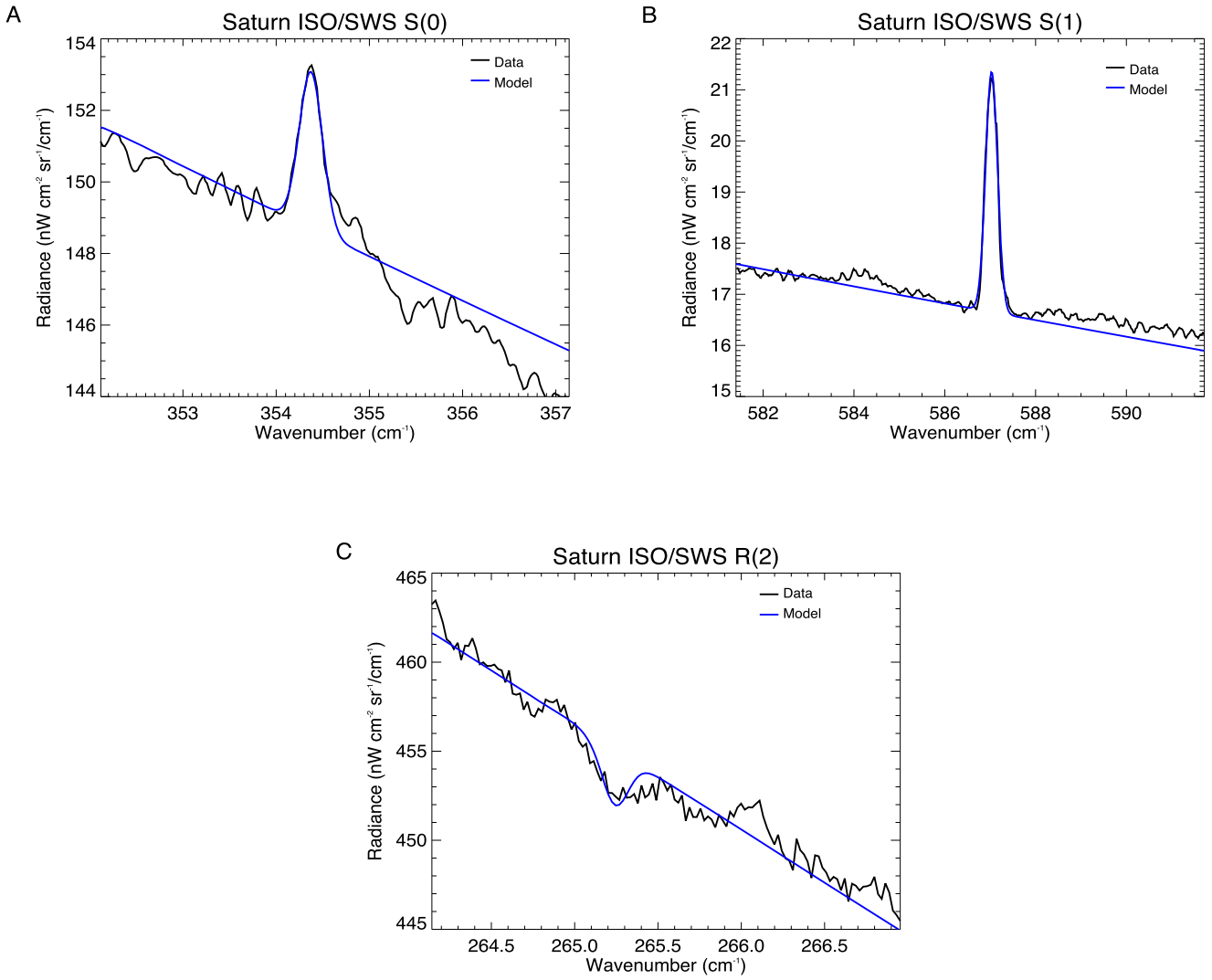

Figure 7. *ISO*/SWS data (black) and NEMESIS model (blue) of the S(0) and S(1) quadrupole lines at 354.37 cm^{-1} (A) and 587.03 cm^{-1} (B), respectively, as well as the R(2) rotational transition absorption visible at 265.24 cm^{-1} (C). The fits are very similar to that of L01 using comparable HD abundances (This work: $[HD] = 2.86 \times 10^{-5}$, L01: $[HD] = 2.98 \times 10^{-5}$ $[HD/H_2 = 3.4 \times 10^{-5}]$, Lellouch et al. 2001).

Table 3
The Original Line Parameters from L01 Used to Confirm That NEMESIS Can Reproduce the Results Found in L01

Line	ν^a (cm^{-1})	Line Intensity (cm^{-1}/(molec cm^{-2}))	γ (cm^{-1}/atm)	E_{Lower} (cm^{-1})	n	δ (cm^{-1}/atm)
R(2)	265.241119	9.002×10^{-24}	0.011	267.070	0.70	0.011

Note. The newer line parameters used in the CIRS analysis derived in Feuchtgruber et al. (2013), seen in Table 2, were then used in a second analysis of the *ISO* data, so that the *ISO* and CIRS results would be directly comparable.

Gautier 2000; $CH_4/H_2 = (4.7 \pm 0.2) \times 10^{-3}$, Fletcher et al. 2009b) used in Equation (2) to calculate a final value of $D/H = (2.10 \pm 0.13) \times 10^{-5}$. The results of this analysis as a function of latitude can be seen in Table 4 (PH_3, NH_3, CH_4, and HD abundances) and Figure 8 (D/H abundance), and a final value of $D/H = (2.10 \pm 0.13) \times 10^{-5}$ was calculated using Equation (3).

In addition, a fractionation factor of 1.34 ± 0.19 (Lellouch et al. 2001) was used to calculate an inferred D/H in CH_4 of $(2.82^{+0.60}_{-0.55}) \times 10^{-5}$, which is relatively high but in agreement with previous measurements of D/H in CH_3D (Figure 9, Fletcher et al. 2009b).

4.1.2. Jupiter

The fit of the NEMESIS model to Jupiter CIRS FP1 data is not as ideal as the fits achieved using Saturn CIRS data, which is expected, as we are modeling a non-homogeneous spectral average using a single temperature and gas profile, leading to a corresponding increase in systematic model error. However, the final value of $D/H = (2.95 \pm 0.55) \times 10^{-5}$ is retrieved for Jupiter,

Table 4
Phosphine, Ammonia, and HD Retrieved Abundances, As Well As the Fractional Scale Height Modeling Parameter (*f;* Equation (1)) for Phosphine and Ammonia on Saturn

Latitude	PH_3 Abundance (ppm, $p > 550$ mbar)	PH_3 f. s.h.	NH_3 Abundance (ppm, $p = 650$ mbar)	NH_3 f. s.h.	HD Mole Fraction ($\times 10^{-5}$) (R(1), 177.84 cm^{-1})
65.5N	6.2 ± 0.06	0.21	0.64 ± 0.017	0.06	3.81 ± 0.40
50.5N	6.1 ± 0.06	0.18	0.37 ± 0.013	0.07	3.96 ± 0.36
41.1N	7.1 ± 0.09	0.19	0.13 ± 0.006	0.08	3.45 ± 0.34
24.2N	13.6 ± 0.27	0.24	0.17 ± 0.010	0.09	3.87 ± 0.35
0.9N	20.1 ± 0.51	0.41	0.17 ± 0.011	0.10	3.69 ± 0.35
13.8S	10.1 ± 0.16	0.35	0.11 ± 0.004	0.08	3.60 ± 0.34
56.6S	5.7 ± 0.04	0.18	0.20 ± 0.004	0.06	3.39 ± 0.32
Global	6.26 ± 0.03	0.25	0.17 ± 0.002	0.08	3.69 ± 0.24
Jupiter	···	0.35	···	0.12	5.17 ± 0.96

Note. In addition, Jupiter fractional scale height (f.s.h.) modeling parameter and HD abundance results are also shown. All trace gas abundances and f.s.h. parameters are in good agreement with previously published values (Irwin et al. 2004; Fletcher et al. 2009a; Hurley et al. 2012). For more information on the HD abundance comparison with previous work, see Section 4.3.2.

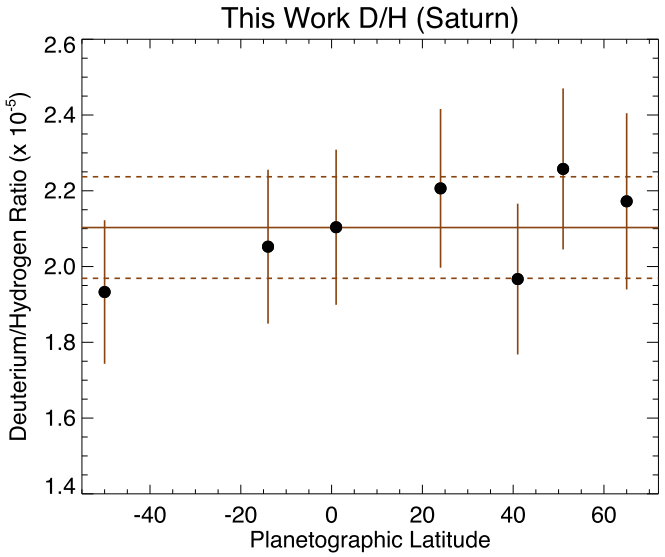

Figure 8. Measured D/H on Saturn at multiple latitudes, with the global mean value and error indicated by solid and dashed horizontal lines. All results agree within error bars, suggesting that deuterium is well-mixed in latitude.

is in excellent agreement with previous determinations (see Section 4.3.2). The error calculation includes the spectral fitting error bar calculated by NEMESIS, the uncertainty in the line intensities given by Feuchtgruber et al. (2013), and the uncertainty in the hydrogen abundance ($He/H_2 = 0.1359 \pm 0.0027$, Von Zahn et al. 1998 $CH_4/H_2 = (2.1 \pm 0.4) \times 10^{-3}$, Niemann et al. 1998) used in Equation (2).

4.2. ISO/SWS

As stated in Section 3.2, the original L01 analysis utilized a range of thermal profiles for Saturn, the results of which are compared against our reanalysis that used the L01 cloud-free, nominal thermal profile in Table 5.

The result of our *ISO* Saturn analysis: $D/H = (1.62 \pm 0.61) \times 10^{-5}$, agrees to within 5% with the previous L01 cloud-free determination: $D/H = (1.70^{+0.78}_{-0.55}) \times 10^{-5}$ (Table 5, Figure 10). This result verifies that the lower D/H in Saturn relative to Jupiter found by the new CIRS analysis is not the consequence of the retrieval algorithm. After we confirmed the accuracy of the NEMESIS model, the *ISO*/SWS data were reanalyzed using the updated line parameters from Feuchtgruber et al. (2013) with the result $D/H = (2.63 \pm 0.82) \times 10^{-5}$. Once again, this work used the cloud-free, nominal thermal profile from L01.

Table 5
A Summary of the Measurements Made by L01 and the Result of This Reanalysis, All Using the Old Line Parameters Described in Table 3

Reference	Cloud Opacity (τ)	Thermal Profile Scaling	Measured D/H ($\times 10^{-5}$)
L01	1.0	0%	$2.00^{+0.92}_{-0.65}$
L01	0.0	−15%	$1.90^{+0.87}_{-0.62}$
L01	0.0	+15%	$1.50^{+0.69}_{-0.49}$
L01	0.0	0%	$1.70^{+0.78}_{-0.55}$
This Work	0.0	0%	1.62 ± 0.61

Note. Shaded in gray are the directly comparable results from L01 and this work, which both used the cloud-free ($\tau = 0$) and neutral (Scale Factor = 0%) thermal profile derived by L01. The final result in L01: $D/H = (1.85^{+0.85}_{-0.60}) \times 10^{-5}$, is an average of the cloud-free and $\tau = 1$ cases.

4.3. Discussion

4.3.1. HD Line Parameters

It should be noted that the line parameters used in the CIRS work are those derived in Feuchtgruber et al. (2013). These values disagree somewhat with those of other databases including HITRAN (Rothman et al. 2013) and CDMS (Müller et al. 2005), leading to a slightly higher measured D/H. Therefore, these results are dependent upon the accuracy of the HD line parameters used in the NEMESIS radiative transfer model.

4.3.2. Measurements

The Saturn $(2.10 \pm 0.13) \times 10^{-5}$ and Jupiter $(2.95 \pm 0.55) \times 10^{-5}$ values agree with previous estimates within error bars, but the new Saturn value is now much more accurate. The Saturn D/H result from CIRS agrees with the original L01 *ISO*/SWS value of $D/H = (1.85^{+0.85}_{-0.60}) \times 10^{-5}$, given the lower signal-to-noise

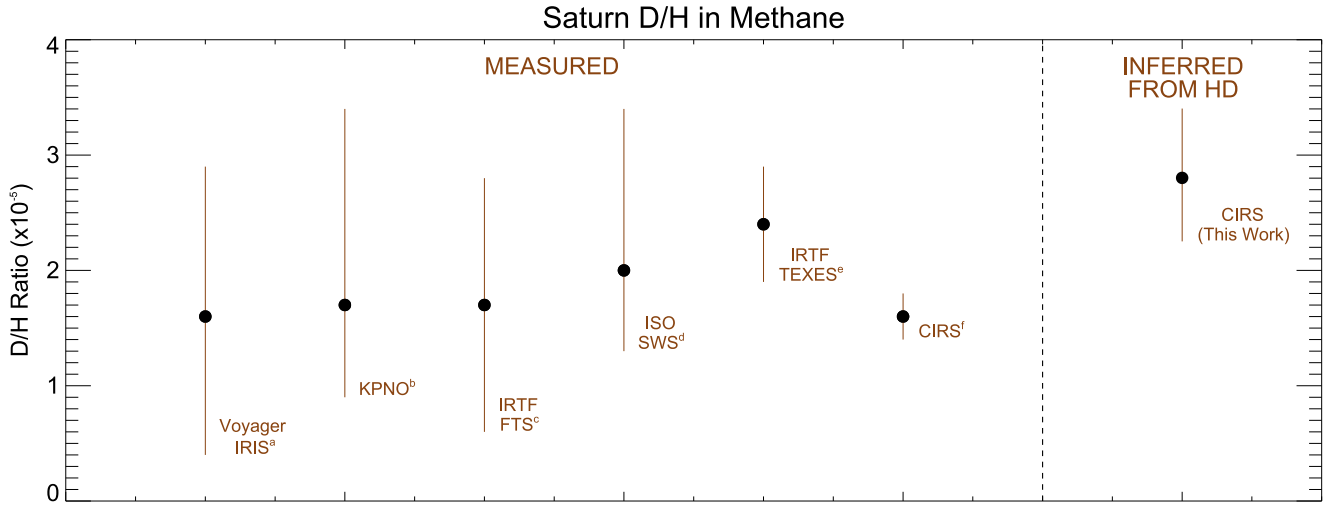

Figure 9. Previous determinations for the D/H in CH_4 on Saturn, as well as the value inferred from the current CIRS results for D/H in H_2 using a fractionation factor $f = 1.34 \pm 0.19$ (Lellouch et al. 2001). This new inferred value, "CIRS (This Work)," is somewhat larger, though still in agreement with previous measurements. (a) Courtin et al. (1984), (b) Owen et al. (1986), (c) Noll & Larson (1991), (d) Lellouch et al. (2001), (e) Bézard et al. (2003), (f) Fletcher et al. (2009).

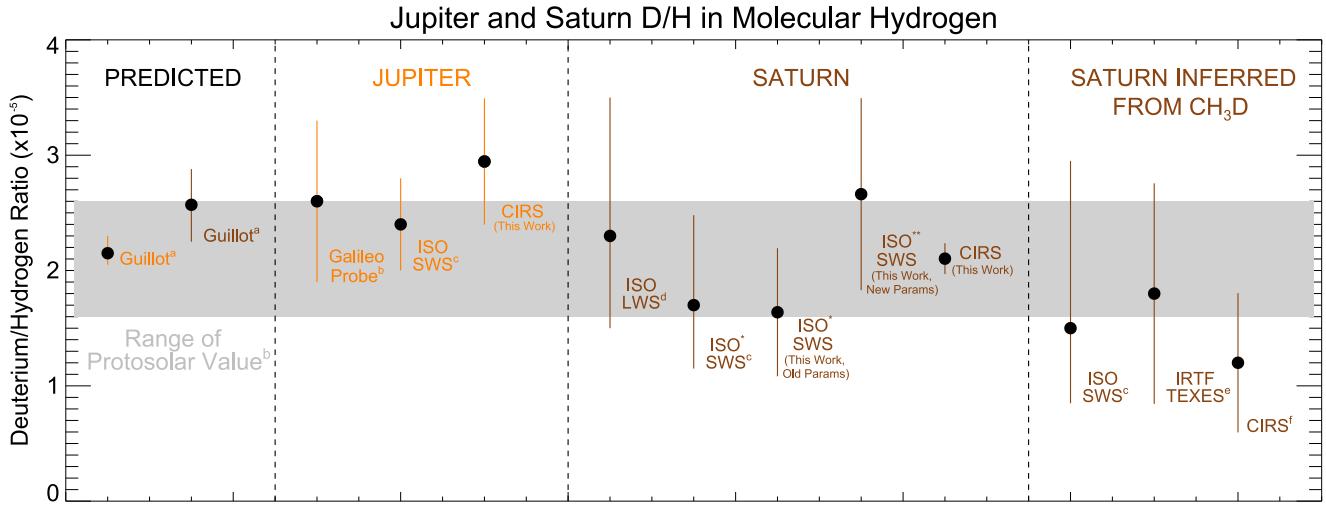

Figure 10. Results from our analysis for D/H in H_2 on Jupiter and Saturn, compared to previous measurements, as well as inferred values from CH_3D using a fractionation factor $f = 1.34 \pm 0.19$ and predicted D/H ratios from Guillot (1999a) or Guillot (1999b). The gray shaded region represents the current knowledge of the protosolar value from meteoritic ^{3}He. The *ISO*/SWS value shown is the cloud-free nominal case, which is directly comparable to the our *ISO* reanalysis (Cloud-Free case with L01 derived line parameters, see Sections 3.3 and 4.2 for details) that used the old line parameters. As a direct comparison with the CIRS result is difficult when different line parameters are used, a third *ISO*/SWS measurement (Cloud-Free case with Feuchtgruber et al. derived line parameters.) was made using the updated line parameters and cloud-free, nominal thermal profile. The new CIRS measurement is well within the error bars of this updated result. For more information on the variety of measurements made by L01, see Sections 3.3 and 4.2. (a) Guillot (1999a), (b) Mahaffy et al. (1998), (c) Lellouch et al. (2001), (d) Griffin et al. (1996), (e) Bézard et al. (2003), (f) Fletcher et al. (2009).

Table 6
Measurements of D/H Ratio on Jupiter and Saturn from CH_4 and H_2, Both Historically and from This Work

H_2			CH_4			
Saturn	Jupiter	Saturn/Jupiter	Saturn	Jupiter	Saturn/Jupiter	References
…	…	…	$1.7^{+1.7}_{-0.8}$	…	…	Owen et al. (1986)
…	…	…	…	2.4 ± 0.7	…	Bjoraker et al. (1986)
…	…	…	2.1 ± 1.3	…	…	Noll & Larson (1991)
$2.3^{+1.2}_{-0.8}$	…	…	…	…	…	Griffin et al. (1996)
…	2.6 ± 0.7	…	…	…	…	Mahaffy et al. (1998)
$1.85^{+0.85}_{-0.6}$	2.4 ± 0.4	$0.77^{+0.6}_{-0.4}$	$2.0^{+1.4}_{-0.7}$	2.2 ± 0.7	$0.91^{+1.4}_{-0.5}$	Lellouch et al. (2001)
…	…	…	1.6 ± 0.2	…	…	Fletcher et al. (2009)
2.10 ± 0.13	2.95 ± 0.55	$0.71^{+0.22}_{-0.15}$	…	…	…	This work (CIRS)

Note. The measured Saturn/Jupiter ratios are shown where possible.

ratio and higher uncertainties in the *ISO*/SWS data including: absolute flux calibration, unknown slope of the continuum, continuum leakage, and a single global temperature profile (Moses et al. 2000; Lellouch et al. 2001). In addition, the result of using the updated line parameters to measure D/H from the *ISO*/SWS data is $D/H = (2.63 \pm 0.82) \times 10^{-5}$, which agrees with the CIRS value within error bars. Figure 10 and Table 6 compare the final results from this work to previous measurements of D/H on Jupiter and Saturn.

The Saturn D/H ratio from CIRS is significantly lower than the measured Jupiter value and is consistent with published protosolar values (Figures 2(B), 10). While the possibility of a lower D/H on Saturn than on Jupiter has been discussed in the past (Lellouch et al. 2001; Fletcher et al. 2009b), no distinction between the two planets could be made given the substantial error bars. Here, we calculate a Saturn/Jupiter D/H ratio of $0.71^{+0.22}_{-0.15}$ using the D/H measured in this work on Jupiter of $(2.95 \pm 0.55) \times 10^{-5}$. While this value is in agreement with previous measurements of this ratio (Table 6), it is in contrast with theoretical expectations, namely a Saturn/Jupiter D/H ratio of ∼1.20 according to interior models of Guillot (Guillot 1999a) and ∼1.05 according to Owen and Encrenaz (Owen & Encrenaz 2006, Figure 10). The result from this work is therefore the strongest evidence so far of a lower D/H ratio on Saturn than Jupiter, an implication with consequences to our understanding of Saturn's internal structure, as well as other planetary and solar system formation. This work is also the first to reach sufficient precision to confirm that the D/H ratio on Saturn falls well within the limits of estimates of the protosolar D/H, as expected.

5. Conclusions

The cause of the lower D/H on Saturn than on Jupiter is unknown—no current theory predicts that outcome. There are four possibilities we can consider: (i) Saturn formed with a lower D/H than Jupiter; (ii) there was subsequent preferential loss of deuterium over hydrogen, and more strongly on Saturn; (iii) sequestration of deuterium from hydrogen into heavy molecules (methane, water, etc.); (iv) phase separation of HD or D_2 inside the giant planets, sequestering deuterium into the core. Regarding (i), there is no widely accepted model where Saturn forms closer to the Sun than Jupiter, allowing for a higher gas fraction. For (ii), we know of no mechanism that would cause preferential loss of the heavier isotope since formation. Atmospheric escape would cause the reverse, and the giant planets are too small to initiate fusion. (iii) appears ruled out by observations: to sequester significant amounts of deuterium from hydrogen into methane (0.4% mole fraction) would very substantially elevate the D/H in methane, which is in conflict with observations (Figure 10). This leaves only (iv), which would predict a presently unknown process. An interesting parallel finding is the possible depletion of helium on Saturn relative to Jupiter, currently explained by a separation of helium droplets from metallic hydrogen leading to a reduced helium abundance in the observable atmosphere (Atreya et al. 1999; Morales et al. 2013; Guillot & Gautier 2015). Note that evolution models also require a much stronger separation of helium on Saturn than on Jupiter to explain their current luminosities. It has been proposed qualitatively that deuterium may be subject to a similar differentiation (Lellouch et al. 2001), presenting a possible explanation for the diminished D/H in the atmosphere of Saturn relative to Jupiter and protosolar. A quantitative assessment of its plausibility remains to be done. If a new process is indeed at work, this would have important implications for our understanding of planetary formation and evolution, in our solar system and other planetary systems. Answering these fundamental questions warrants further investigation into the deuterium and helium abundances of both giant planets, and strengthens the case for a Galileo-like probe to Saturn to perform in situ measurements (Mousis et al. 2014).

The US-based authors: J.E.D.P., C.A.N., G.L.B., R.K.A., B.E.H., and F.M.F. were supported by the NASA *Cassini* Mission during the period when this research was conducted. L.N.F. was supported by a Royal Society Research Fellowship at the University of Leicester. P.G.J.I. was supported by the United Kingdom Science and Technology Facilities Council.

ORCID iDs

C. A. Nixon https://orcid.org/0000-0001-9540-9121
E. Lellouch https://orcid.org/0000-0001-7168-1577
L. N. Fletcher https://orcid.org/0000-0001-5834-9588
G. L. Bjoraker https://orcid.org/0000-0002-9679-4153
B. Bézard https://orcid.org/0000-0002-5433-5661
P. G. J. Irwin https://orcid.org/0000-0002-6772-384X

References

Achterberg, R. K., Gierasch, P. J., Conrath, B. J., et al. 2014, ApJ, 92, 92
Atreya, S. K., Wong, M. H., Owen, T. C., et al. 1999, P&SS, 47, 1243
Bézard, B., Greathouse, T., Lacy, J., Richter, M., & Griffith, C. A. 2003, BAAS, 35, 1017
Bjoraker, G. L., Larson, H. P., & Kunde, V. G. 1986, Icar, 66, 579
Chan, C., Albright, S., Gorius, N., et al. 2015, ExA, 39, 367
Conrath, B., & Gautier, D. 2000, Icar, 144, 124
Courtin, R., Gautier, D., Marten, A., Bezard, B., & Hanel, R. 1984, ApJ, 287, 899
Ferlet, R., & Lemoine, M. 1998, SSRv, 84, 297
Feuchtgruber, H., Lellouch, E., Orton, G., et al. 2013, A&A, 551, A126
Flasar, F. M., Kunde, V. G., Abbas, M. M., et al. 2004, SSRv, 115, 169
Fletcher, L. N. 2007, D. Phil. thesis, Jesus College
Fletcher, L. N., Achterberg, R. K., Greathouse, T. K., et al. 2010, Icar, 208, 337
Fletcher, L. N., Greathouse, T. K., Orton, G. S., et al. 2014, Icar, 238, 170
Fletcher, L. N., Orton, G. S., Teanby, N. A., & Irwin, P. G. J. 2009a, Icar, 202, 543
Fletcher, L. N., Orton, G. S., Teanby, N. A., Irwin, P. G. J., & Bjoraker, G. L. 2009b, Icar, 199, 351
Geiss, J., & Gloecker, G. 1998, SSRv, 84, 239
Griffin, M. J., Naylor, D. A., Davis, G. R., et al. 1996, A&A, 315, 389
Guillot, T. 1999a, P&SS, 47, 1183
Guillot, T. 1999b, Sci, 286, 72
Guillot, T., & Gautier, D. 2015, Treatise on Geophysics (2nd ed.; Amsterdam: Elsevier)
Hersant, F., Gautier, D., & Huré, J. 2001, ApJ, 554, 391
Hurley, J., Fletcher, L. N., Irwin, P. G. J., et al. 2012, P&SS, 73, 347
Irwin, P. G. J., Parrish, P., Fouchet, T., et al. 2004, Icar, 172, 37
Irwin, P. G. J., Teanby, N. A., de Kok, R., et al. 2008, JQSRT, 109, 1136
Jennings, D. E., Flasar, F. M., Kunde, V. G., et al. 2017, ApOpt, 56, 5274
Lacis, A., & Oinas, V. 1991, JGR, 96, 9027
Lellouch, E., Bezard, B., Fouchet, T., et al. 2001, A&A, 370, 610
Linsky, J. L. 1998, SSRv, 84, 285
Mahaffy, P. R., Donahue, T. M., Atreya, S. K., Owen, T. C., & Niemann, H. B. 1998, SSRv, 84, 251

Morales, M. A., Hamel, S., Caspersen, K., & Schwegler, E. 2013, PhRvB, 87, 174105
Moses, J. I., Bezard, B., Lellouch, E., et al. 2000, Icar, 143, 244
Mousis, O., Fletcher, L. N., Lebreton, J. P., et al. 2014, P&SS, 104, 29
Müller, H. S. P., Schlöder, F., Stutzki, J., & Winnewisser, G. 2005, JMoSt, 742, 215
Niemann, H. B., Atreya, S. K., Carignan, G. R., et al. 1998, JGR, 103, 22831
Nixon, C. A., Achterberg, R. K., Conrath, B. J., et al. 2007, Icar, 188, 47
Nixon, C. A., Achterberg, R. K., Romani, P. N., et al. 2010, P&SS, 58, 1667
Noll, K. S., & Larson, H. P. 1991, Icar, 89, 168
Owen, T., & Encrenaz, T. 2006, P&SS, 54, 1188
Owen, T. C., Lutz, B. L., & de, B. C. 1986, Natur, 320, 244
Rothman, L. S., Gordon, I. E., Babikov, Y., et al. 2013, JQSRT, 130, 4
Von Zahn, U., Hunten, D. M., & Lehmacher, G. 1998, JGR, 103, 22815